In vivo and postmortem memory circuit integrity in frontotemporal dementia and Alzheimer's disease

Author:
Hornberger, Michael; Wong, Stephanie; Tan, Rachel; Irish, Muireann; Piguet, Olivier; Kril, Jillian; Hodges, John R; Halliday, Glenda

Publication details:
Brain
v. 135
Chapter No. Pt 10
pp. 3015-3025
0006-8950 (ISSN)

Publication Date:
2012

Publisher DOI:
http://dx.doi.org/10.1093/brain/aws239

Title: *In vivo* and postmortem memory circuit integrity in frontotemporal dementia and Alzheimer's disease

Authors: Hornberger, M.[1,2,3], PhD, Wong, S., BPsych(Hons) [1], Tan, R., PhD[1], Irish, M., PhD[1,2,3], Piguet, O., PhD[1,2,3], Kril, J., PhD FFSc (RCPA)[4], Hodges, J.R., MD, FRCP [1,2,3], Halliday, G., PhD[1,2,3]

[1] Neuroscience Research Australia, Sydney, Australia

[2] School of Medical Sciences, University of New South Wales, Sydney, Australia

[3] ARC Centre of Excellence in Cognition and its Disorders, Sydney, Australia

[4] Disciplines of Medicine and Pathology, Sydney Medical School, The University of Sydney

Corresponding author:

Dr. Michael Hornberger

Neuroscience Research Australia,

PO Box 1165

Sydney, Australia

Tel. +61 2 9399 1816

Fax. +61 2 9399 1047

Email: m.hornberger@neura.edu.au

Running title: Papez memory circuit in bvFTD and AD

Words in abstract: 239 **Words in manuscript:** XXX

Tables: 2 **Figures:** 4 (3 colour figures)

Supplementary Table: 1

Abstract

Behavioural variant frontotemporal dementia (bvFTD) can present with episodic memory deficits as severe as those in Alzheimer's disease (AD). Little is known of the integrity of grey matter areas and white matter tracts of the Papez memory circuit in these diseases. The integrity of the Papez circuit (hippocampus, fornix, mammillary bodies, anterior thalamus, cingulate cortex) was investigated *in vivo* and at *postmortem* in bvFTD and AD cohorts using voxel-based morphometry, diffusion tensor imaging and manual volumetric tracing. Our findings indicate that bvFTD and AD show similar degrees of hippocampal atrophy *in vivo*, but bvFTD patients show greater hippocampal atrophy at *postmortem,* with the FTLD-TDP subtype being particularly affected. Cingulate cortex findings show an expected atrophy pattern with bvFTD being affected more anteriorly and AD showing more posterior atrophy. More importantly, subcortical Papez circuit regions (fornix and anterior thalamus) were affected in bvFTD only, with atrophy in these regions determining the degree of amnesia in bvFTD. Hippocampal atrophy does not appear to be an efficient diagnostic marker for underlying bvFTD or AD pathology, although for bvFTD, episodic memory deficits in conjunction with marked hippocampal atrophy emerge as potential biomarkers for FTLD-TDP pathology. Subregions of Papez circuit were differentially affected in bvFTD and AD with subcortical regions determining the degree of episodic memory deficits in bvFTD. Subcortical atrophy should be taken into account when establishing whether the severe amnesia observed in a patient is likely due to bvFTD or AD pathology.

Key words: behavioural variant frontotemporal dementia, Alzheimer's disease, episodic memory, Papez circuit

Introduction

The medial temporal lobe, particularly the hippocampus, is widely regarded as the key memory related region as its surgical removal has severe effects on memory performance (Milner and Penfield, 1955). The hippocampus is one of the earliest regions to degenerate in Alzheimer's disease (AD) (Braak and Braak, 1991a) and episodic memory deficits, a well-established early feature of AD (McKhann *et al.* , 1984), are usually attributed to hippocampal pathology (de Leon *et al.* , 1996, Jack *et al.* , 1997). Mounting evidence shows that patients with behavioural-variant frontotemporal dementia (bvFTD) also experience episodic memory impairment which, in some cases, may be of similar severity to that seen in AD (Graham *et al.* , 2005, Hornberger *et al.* , 2010). At present, little is known about the integrity of the episodic memory systems in bvFTD, although considerable *postmortem* pathology occurs in the hippocampus in bvFTD, even in patients dying early in the course of the disease (Broe *et al.* , 2003, Kril and Halliday, 2004). Medial temporal lobe atrophy has also been reported in bvFTD using neuroimaging (Rabinovici *et al.* , 2007, Seeley *et al.* , 2008, Whitwell *et al.* , 2009). Whilst initial studies reported a greater hippocampal atrophy in AD than bvFTD (Boccardi *et al.* , 2003, Grossman *et al.* , 2004), recent studies show a similar degree of hippocampal atrophy in bvFTD and AD (Rabinovici *et al.* , 2007, van de Pol *et al.* , 2006), as well as in surrounding cortices (entorhinal and perirhinal) (Pennington *et al.* , 2011).

Importantly, the hippocampus is but one region in a larger memory circuit, the so-called "Papez circuit" (Figure 1), which comprises hippocampus, fornix, mammillary bodies, anterior thalamus and cingulate cortex. Lesions affecting any region of the Papez circuit produce substantial memory deficits in animals and humans, even when sparing the hippocampus (for a review see Aggleton and Brown, 1999). Neuroimaging and neuropathological investigations have shown that all Papez circuit regions degenerate in AD, except the anterior cingulate

Glenda Halliday 9/6/12 8:11 PM
Deleted: (

Glenda Halliday 9/6/12 8:11 PM
Deleted:)

(Callen *et al.* , 2001, Hooper and Vogel, 1976), with hippocampal and posterior cingulate regions being particularly affected. In contrast, studies of bvFTD atrophy have focused exclusively on the hippocampus and cingulate regions, in particular the anterior cingulate cortex (Rabinovici *et al.* , 2007, Seeley *et al.* , 2008). To our knowledge, no study has investigated the integrity of the remaining relay stations of the Papez circuit in bvFTD.

The current study investigated whether Papez circuit grey matter regions (hippocampus, mammillary bodies, anterior thalamus, cingulate cortex) and the main white matter tract (fornix) are differentially atrophied in bvFTD and AD. We employed parallel *in vivo* and *postmortem* volumetric methods to establish the intactness of the circuit with disease progression. For the *in vivo* study, we conducted region of interest voxel-based morphometry and diffusion tensor imaging analyses in a clinical cohort of bvFTD and AD patients compared with controls. To confirm the clinical findings in a *postmortem* sample, we conducted volumetric analysis of grey matter regions of interest in pathologically-verified cases of bvFTD, AD and controls. Based on previous findings, we predicted that both groups would show similar atrophy of the hippocampus, with atrophy of the posterior cingulate cortex more substantial in AD and atrophy of the anterior cingulate cortex more substantial in bvFTD. We also predicted that the fornix, mammillary bodies and anterior thalamus would be atrophic in AD.

Glenda Halliday 9/6/12 8:13 PM
Deleted:

Methods

In vivo cohort

Fifteen patients with a clinical diagnosis of bvFTD (Rascovsky *et al.* , 2011) were recruited from the Frontotemporal Dementia Research Group (FRONTIER) at Neuroscience Research Australia (NeuRA) following study approval by the University of New South Wales Human Research Ethics Advisory panel D (Biomedical, ref. #10035). The bvFTD group was contrasted

with 15 patients with a diagnosis of probable AD (McKhann *et al.* , 1984), as well as 18 healthy controls from the FRONTIER participant database. AD patients and controls were matched for clinical and demographic variables (Table 1) to the bvFTD group. Clinical, neuropsychological and demographics data (Table 1) as well as high-resolution coronal T1 and diffusion tensor MR brain images were available for all participants. All participants underwent comprehensive neuropsychological testing, including the following episodic memory tests: Rey Auditory Verbal Learning Test (RAVLT) immediate recall after an interference list (A6) and recognition after 30 minutes. Visual recall was investigated with the Rey-Osterrieth Complex Figure Test (RCF) and visual recognition with the Doors and People test (part A). Patients were all tested and scanned at the first clinic presentation.

Postmortem cohort

Nineteen cases with a clinical diagnosis of bvFTD (Rascovsky *et al.* , 2011) and FTLD pathology (Mackenzie *et al.* , 2010), 18 cases with clinical and pathological AD (Mirra *et al.* , 1991) (Braak and Braak, 1991b), and 20 controls without dementia or significant neuropathological abnormalities were selected from a neuropathological series of cases collected by the Sydney Brain Bank through a regional brain donor program in Sydney, Australia. The program holds approval from the Human Ethics Committees of the Central and South Eastern Sydney Area Health Services and The Universities of Sydney and New South Wales and complies with the statement on human experimentation issued by the National Health and Medical Research Council of Australia. Some cases have previously been reported (Halliday *et al.* , 2003, Kril *et al.* , 2005). Diagnostic clinical, neuropathological and demographic data (Table 1) as well as high-resolution coronal photos of 3mm brain slices were available for all participants. All dementia cases had Clinical Dementia Rating (CDR) scores between 1 and 3 while controls had scores of <0.5). The *postmortem* interval was 22 hours on average (range: 2-68 h; mean ±SD for control=22±13, for AD=21±15, and for bvFTD=17±16,

Glenda Halliday 10/4/14 9:53 AM
Comment: Fix separate refs?

F=1.417, p=0.25). Based on immunohistochemical inclusions, bvFTD cases were further classified as having TDP pathology (n=9, 6 males; age range 53-82 years; 6 with type A and 3 with type B, Mackenzie *et al.* 2011) or tau pathology (n=10, 3 males; age range 65-82 years; 7 with Pick's disease and 3 with corticobasal degeneration).

Glenda Halliday 10/4/14 9:53 AM
Comment: Acta Neuropathol. 2011 Jul;122(1):111-3. Epub 2011 Jun 5.
A harmonized classification system for FTLD-TDP pathology.
Mackenzie IR, Neumann M, Baborie A, Sampathu DM, Du Plessis D, Jaros E, Perry RH, Trojanowski JQ, Mann DM, Lee VM.

In vivo cohort - MRI acquisition and analyses

Imaging acquisition

All patients and controls in the clinical cohort underwent the same imaging protocol with whole-brain T1 and DTI-weighted images using a 3T Philips MRI scanner with standard quadrature head coil (8 channels). The 3D T1-weighted sequences were acquired as follows: coronal orientation, matrix 256x256, 200 slices, 1x1mm^2 in-plane resolution, slice thickness 1mm, TE/TR=2.6/5.8ms. The DTI-weighted sequences were acquired as follows: 32 gradient direction diffusion tensor imaging (DTI) sequence (TR/TE/TI: 8400/68/90ms; b-value = 1000s/mm^2; 55 2.5mm horizontal slices, end resolution: 2.5x2.5x2.5mm^3; field of view 240x240 mm, 96x96 matrix; repeated 2 times). Two DTI sequences were acquired for each participant, which were in a first step then averaged and corrected for eddy current distortions. The diffusion tensor models were then fitted at each voxel via the FDT toolbox in FSL (http://www.fmrib.ox.ac.uk/fsl/fdt/index.html), resulting in maps of three eigenvalues (L1, L2, L3) which allowed calculation of fractional anisotropy (FA) maps for each subject.

Glenda Halliday 9/6/12 8:12 PM
Deleted:

Glenda Halliday 9/6/12 8:12 PM
Deleted:

Voxel-based morphometry (VBM) analysis

3D T1-weighted sequences were analysed with FSL-VBM, a voxel-based morphometry analysis(Ashburner and Friston, 2000, Good *et al.* , 2001) which is part of the FSL software package http://www.fmrib.ox.ac.uk/fsl/fslvbm/index.html. First, tissue segmentation was carried out using FMRIB's Automatic Segmentation Tool (FAST) from brain extracted images. The resulting gray matter partial volume maps were then aligned to the Montreal Neurological

Institute standard space (MNI152) using the nonlinear registration approach using FNIRT, which uses a b-spline representation of the registration warp field. The registered partial volume maps were then modulated (to correct for local expansion or contraction) by dividing them by the Jacobian of the warp field. The modulated images were then smoothed with an isotropic Gaussian kernel with a standard deviation of 3mm (FWHM: 8mm). A voxelwise general linear model (GLM) was applied and permutation-based non-parametric testing was used to form clusters with the Threshold-Free Cluster Enhancement (TFCE) method, tested for significance at $p<0.001$, uncorrected with a voxel threshold of at least 20 contiguous voxels. Finally, regions of interests for the hippocampus, mammillary bodies, thalamus and cingulate were created by generating masks based on the Harvard-Oxford cortical and subcortical probabilistic atlases (Desikan *et al.* , 2006).

Diffusion tensor imaging (DTI) analysis

Tract-Based Spatial Statistics (TBSS) from FSL were used to perform a skeleton-based analysis of white matter FA. FA maps of each individual subject were eddy current corrected and co-registered using nonlinear registration using FNIRT to the MNI standard space using the FMRIB58_FA template, which is available as part of the FSL software. The template was subsampled at $2x2x2mm^3$ due to the coarse resolution of native DTI data (i.e. $2.5x2.5x2.5mm^3$). After image registration, FA maps were averaged to produce a group mean FA image. A skeletonization algorithm was applied to the group mean FA image to define a group template of the lines of maximum FA, assumed to correspond to centers of white matter tracts. FA values for each individual subject were then projected onto this group template skeleton. Clusters were tested using permutation-based non-parametric testing as described for the VBM analysis. Clusters reported have significance at $p<0.05$, corrected for multiple comparisons across via family-wise error correction space, unless otherwise stated. Similar to the VBM analysis, masks

for the regions of interest (fornix, cingulate cingulum) were created based on the probabilistic JHU White-Matter Tractography Atlas (Mori *et al.* , 2005).

Glenda Halliday 9/6/12 8:12 PM
Deleted:

Postmortem preparation and volume analyses

Brain preparation

The volumetric methods used in this study have been published in detail elsewhere (Halliday *et al.* , 2003). Briefly, following 14-day fixation in 15% neutral buffered formalin, each brain was weighed and the volume determined by fluid displacement. The cerebellum and brainstem were separated from the cerebrum by sectioning through the cerebral peduncles. Each cerebrum was embedded in 3% agar and sectioned in 3mm coronal slices. Slices were photographed and printed at 1× magnification. Average slice thickness for each brain was determined by dividing the hemisphere length by the total number of slices.

The regions of interest (hippocampus, mammillary bodies, thalamus and cingulate) were quantified in the left and right hemispheres of each brain. In accordance with human brain atlases, gyral boundaries and anatomical structures most consistently associated with cytoarchitectonic boundaries were used to identify regions across all cases.

Hippocampus - The anterior border of the hippocampus is determined by the alveus, which separates the hippocampus from the amygdala. Its posterior limit is where the hippocampal ovoid grey matter entirely disappears. The CSF of the lateral ventricle is used as an external marker for the lateral border of the hippocampus. The superior and inferior borders of the hippocampus are defined by the alveus and white matter of the parahippocampal gyrus, respectively.

Mammillary bodies - The mammillary bodies are two spherical structures that lie inferior to the hypothalamus and anterior to the crus cerebri. The lateral border is defined by connecting the points of the ‘mammillary notches’.

Anterior thalamus - The anterior tubercle of the thalamus lies posterior to the interventricular foramen and anterior commissure. The superior border of the anterior thalamus forms part of the floor of the lateral ventricles. It is laterally and inferiorly bound by the internal medullary lamina. The anterior thalamus narrows towards its posterior pole, which occurs where the anterior tubercle no longer protrudes from the superior border of the thalamus.

Cingulate Cortex – was defined as the cortex in the cingulate gyrus surrounding the corpus callosum and defined by the cingulate sulcus. The anterior cingulate cortex includes subgenual and pregenual regions as well as cingulate cortex above the corpus callosum in coronal slices anterior to the pallidum. The posterior cingulate cortex was determined as the cingulate cortex posterior to the central lobule of the central sulcus and commenced in coronal slices posterior to the pallidum.

Volume determination

The volumes of the regions of interest were determined by a point counting procedure with two raters used to identify regions of interest and determine volumes. The areas corresponding to each region were identified on the brain slice photographs, which were randomly overlaid with a grid of 3848 points (each separated by 4mm). The total number of points falling on each region of interest was counted. Volumes were calculated by multiplying the sum of the points falling on a given structure by the volume represented by each point (volume/point=16mm^2 × mean slice thickness; average of 50mm^3). The raters were initially trained to identify the same regions of interest in three brains with less than 5% variation. The raters were considered competent where less than 5% variation was obtained in 10 repeated measures of the regions of interest in 3 cases. Two independent raters traced the regions of interest in 3 cases with a correlation between counts of 0.978. The only departure from this method was the volumetric measurement of the mammillary bodies which was traced onto digital images of the brain slice photographs to measure the cross-sectional area. In repeated measurements on 8 cases the main rater had <2%

Glenda Halliday 9/6/12 8:14 PM
Deleted:

variation. Two independent raters traced the regions of interest in 8 cases with a correlation between measures of 0.988. Volumes of the mammillary bodies were calculated using Cavalieri's principle (area of region of interest × mean slice thickness).

Quantitation of hippocampal inclusions

Sections of the hippocampus immunohistochemically stained with TDP-43 (rabbit anti-human TDP-43 diluted 1: 800; ProteinTech, Chicago, IL, USA) and tau (mouse anti-human tau diluted 1:1000; Thermo Scientific, Scoresby, VIC, Australia) antibodies were evaluated for each case. Systematic sampling of the same anatomical regions of both the CA1 region and dentate gyrus were used. For the CA1, the proportion of neurons containing immunohistochemically-identified inclusions were evaluated using standard inclusion and exclusion borders within one 400 x 400µm field located laterally in the mid-CA1 region at the superficial ventricular surface, as previously published (Kersaitis *et al.* 2004). For the dentate gyrus, the proportion of neurons containing immunohistochemically-identified inclusions were evaluated using standard inclusion and exclusion borders within two 200 x 200µm fields located midway along the lateral aspects of the cup-shaped gyrus. A further 200 x 200 µm field containing the highest observable density of immunohistochemically-identified inclusions was also evaluated. There was no difference between two raters in the density of inclusions counted in all cases (paired t-test $P = 0.24$; R = 0.079, $P < 0.0001$). The density measures were standardised to numbers/mm^2.

Glenda Halliday 9/6/12 10:01 PM
Deleted: Histopathological analysis

Glenda Halliday 9/6/12 10:02 PM
Deleted: Hippocampal s

Glenda Halliday 9/6/12 10:02 PM
Deleted: stained

Glenda Halliday 9/6/12 10:02 PM
Deleted: for

Glenda Halliday 9/6/12 10:13 PM
Formatted: Highlight

Glenda Halliday 9/6/12 10:13 PM
Formatted: Highlight

Glenda Halliday 10/4/14 9:53 AM
Comment: Regional and cellular pathology in frontotemporal dementia: relationship to stage of disease in cases with and without Pick bodies.
Kersaitis C, Halliday GM, Kril JJ. Acta Neuropathol. 2004 Dec;108(6):515-23.

Glenda Halliday 9/6/12 10:31 PM
Deleted: More here

Statistical analysis

Data were analysed using SPSS19.0 (IBM Corp., Chicago, Ill., USA). Parametric demographic (age, education, disease duration), clinical (CDR) and general cognitive (ACE-R) and *postmortem* region of interest volumes and hippocampal lesion densities were compared across groups via one-way ANOVAs followed by Tukey post-hoc tests. A priori, variables were

Glenda Halliday 10/6/12 7:59 AM
Deleted: ,

Glenda Halliday 9/6/12 10:45 PM
Formatted: Highlight

Glenda Halliday 10/6/12 8:02 AM
Deleted: the three

Glenda Halliday 10/6/12 8:02 AM
Deleted: (bvFTD, AD and controls)

plotted and checked for normality of distribution by Kolmogorov-Smirnov tests. Variables revealing non-normal distributions were log transformed and the appropriate log values were used in the analyses. Variables showing non-parametric distribution after log transformation were analysed via Chi-square, Kruskal-Wallis and Mann-Whitney U tests. Spearman rank correlations were used to confirm any relationships between regional volumes, hippocampal lesion densities and measures of disease severity (disease stage, duration and CDR score) in the *postmortem* cohort.

Glenda Halliday 9/6/12 10:45 PM
Formatted: Highlight

Results

Demographics & cognitive tests

Demographics and general cognitive scores for the clinical cohort can be seen in Table 1. AD and bvFTD participants in the clinical cohort did not differ in terms of age or sex distribution (all p values > .1), whereas the bvFTD patients in the *postmortem* cohort died at a younger age ($p<.01$) and less advanced pathological disease stage ($p < .001$) than the AD patients. Importantly, bvFTD and AD patients did not differ in disease duration in either cohort ($p>.1$) and had a similar *postmortem* delay in the *postmortem* cohort. On cognitive testing, the clinical patient groups differed significantly on the general cognitive measure (ACE) from controls ($p<.001$) but not from each other ($p>.1$) and the *postmortem* dementia groups also did not differ on their clinical dementia ratings. Similarly, on all memory measures, except the RAVLT recognition score, the clinical bvFTD and AD groups scored significantly lower than controls ($p<.05$), but did not differ from each other ($p>.1$). A split by immunohistochemical inclusions in the *postmortem* cohort revealed that bvFTD cases with both types of TDP pathology, but particularly cases with TDP type A, were younger ($p<.05$), had significantly shorter disease durations ($p<.05$) and were less advanced in disease stage ($p<.01$) than those with both types of tau pathology. Age was used as a covariate in further analyses.

Glenda Halliday 9/6/12 9:58 PM
Formatted: Highlight

Glenda Halliday 9/6/12 9:58 PM
Formatted: Highlight

Glenda Halliday 9/6/12 9:58 PM
Formatted: Highlight

Voxel-based morphometry & Diffusion Tensor Imaging analyses in the clinical cohort

Figures 2 and 3 show that both clinical patient groups (bvFTD, AD) had substantial atrophy of the bilateral hippocampus, fornix and cingulate cortex in comparison to controls, while only bvFTD had atrophy of the left anterior thalamus compared with controls. Analysis of mammillary body volumes revealed no significant results between patients and controls.

A direct contrast of the patient groups revealed no additional hippocampal atrophy for the bvFTD patients in comparison to AD, but more fornix degeneration (Figure 2), left anterior thalamus and bilateral anterior cingulate atrophy (Figure 3) in bvFTD than in AD. The reverse contrast (AD > bvFTD) showed greater right posterior hippocampal atrophy in AD than in bvFTD (Figure 2).

We median split the bvFTD patients of the clinical cohort into high (bvFTD+; n=7) vs. low (bvFTD-; n=8) memory impairment based on their performance on the RAVLT A6 score, which a previous study revealed as one of the most sensitive measures to detect memory deficits in bvFTD(Hornberger *et al.* , 2010). We conducted an a priori power analysis to calculate the minimum sample size to detect group difference based on the RAVLT A6 memory score. The power calculation, based on the previous findings in independent and much bigger patient and control cohorts (bvFTD: n=50; AD: n= 64; controls: n=64) (Hornberger et al. 2010), revealed an effect size of d = 2.56 for the RAVLT A6. Based on this effect size, power calculations revealed that with an α-level of .05 the estimated minimal group sizes to detect significant differences across groups is n=5, which we exceeded in this analysis. Importantly, the bvFTD subgroups (bvFTD+, bvFTD-) did not differ on age or disease severity ($p>.1$). As shown in Figure 4, bvFTD+ patients showed greater atrophy in left posterior hippocampus and left anterior thalamus in comparison to the bvFTD- group. The opposite contrasts revealed no significant

results. More importantly, bvFTD+ patients also differed from AD patients by showing additional atrophy of the left anterior thalamus and bilateral anterior cingulate cortex (Figure 4). By contrast, AD patients showed more atrophy than bvFTD+ patients in the bilateral posterior cingulate cortex.

Postmortem volumetric analyses & hippocampal lesion densities

Significant between-group differences in region of interest volumes were present ($p<.001$). These differences were of similar magnitude in both hemispheres ($p>.1$) and no clinical group by hemisphere interaction was present ($p>.1$). In comparison to controls, all regions were atrophic in the bvFTD cases (average percentage of atrophy in comparison to controls; hippocampus: 45%; mammillary bodies: 33%; anterior thalamus: 39% and cingulate cortex: 40%) (Table 2). Compared with controls, AD cases had significant atrophy of the hippocampus (average 33% atrophy) and cingulate cortex (average 20% atrophy) (Table 2). Overall, the degree of atrophy in the hippocampus and cingulate cortex was significantly worse in bvFTD compared to AD (Table 2), although the cases with corticobasal degeneration had similar hippocampal atrophy to AD (Table 2). Within the bvFTD cohort, those with FTLD-TDP Type A pathology had significantly greater mammillary body atrophy ($p<.01$) and those with FTLD-tau Pick's disease had significantly greater anterior cingulate atrophy ($p<.01$) with no significant differences between bvFTD subgroups in the other regions (Table 2).

Glenda Halliday 10/6/12 10:38 AM
Deleted: 19.5

Glenda Halliday 10/6/12 10:44 AM
Deleted: hippocampal

Glenda Halliday 10/6/12 10:44 AM
Deleted: than those with tau pathology

Significant numbers of neurons had tau-immunoreactive inclusions in the CA1 region of the hippocampus in AD and the bvFTD-tau subgroups (Fig. 5A,B). In contrast, relatively few neuronal inclusions were observed in the CA1 hippocampal region in the bv-FTD-TDP subgroups (Table 3). Higher densities of neuronal inclusions were observed in the dentate gyrus compared with the CA1 region of the hippocampus in all the types of bvFTD cases (Fig. 5C-F). Cases with Pick's disease (PiD) had the highest densities of inclusions in the CA1 and dentate

gyrus of the hippocampus, while cases with AD had the lowest densities of neuronal inclusions in the dentate gyrus (Table 3).

Glenda Halliday 9/6/12 10:55 PM
Formatted: Font:Not Bold

Spearman rank correlations were used to determine any relationships between the severity of inclusion pathology and the degree of hippocampal atrophy using the whole cohort (including controls), AD and bvFTD cases only, or bvFTD cases only. In all instances, there were no correlations between the degree of hippocampal atrophy and the severity of CA1 inclusion pathology. There were correlations between increasing hippocampal atrophy and increasing densities of inclusions in dentate neurons using the entire cohort (Rho>0.45, p<0.0001) or when only AD and bvFTD cases were assessed (Rho>0.25, p<0.03), but not when bvFTD cases were assessed alone (p>0.2).

Glenda Halliday 10/6/12 4:38 PM
Formatted: Font:Not Bold

Spearman rank correlations were used to identify any relationships between *postmortem* regional atrophy or the density of regional hippocampal inclusion pathology and disease stage, disease duration and last CDR score in the AD and bvFTD cases. Atrophy of the hippocampus and cingulate cortices were more pronounced and the severity of dentate inclusion pathology increased with increasing disease duration ($p<.05$) and CDR score ($p<.01$), indicating ongoing degeneration and inclusion pathology over the disease course. To determine the strengths of the associations for disease duration and last CDR score, partial correlations were performed controlling for each of these variables. Increasing atrophy of the hippocampus and anterior cingulate cortex occurred with greater disease durations, controlling for CDR score (p<.05), while increasing posterior cingulate cortex atrophy and higher maximal densities of dentate gyrus inclusions occurred with increasing CRD scores, controlling for disease duration (p<.01). Atrophy of the hippocampus and posterior cingulate cortex was also related to pathological stage ($p<.05$), confirming a relationship between hippocampal pathology and atrophy and indicating a similar relationship with the posterior cingulate cortex.

Glenda Halliday 10/6/12 5:01 PM
Deleted: the total and posterior

Glenda Halliday 10/6/12 5:14 PM
Formatted: Font:Not Italic

Glenda Halliday 10/6/12 5:02 PM
Deleted: indicating

Glenda Halliday 10/6/12 5:05 PM
Deleted: those regions and pathological severity

Discussion

This study is the first to report degenerative changes affecting all relay nodes of the Papez circuit in bvFTD. bvFTD patients with high memory loss had more severe neural degeneration of the fornix, anterior thalamus and anterior cingulate cortex than patients with AD, while patients with AD had more significant atrophy of the posterior cingulate cortex. Hippocampal atrophy was similar for both the bvFTD and AD cohorts, as predicted from previous studies (Broe *et al.* , 2003, Rabinovici *et al.* , 2007, van de Pol *et al.* , 2006); however, over time, atrophy of the hippocampus and posterior cingulate cortex become more severe in bvFTD compared with pathologically-confirmed cases of AD. This novel finding demonstrates that hippocampal and cingulate pathology begin early in bvFTD and progresses more rapidly than in AD. The greater hippocampal atrophy in bvFTD was driven by TDP pathology, consistent with previous findings showing that bvFTD patients with TDP pathology have more subcortical involvement (Piguet *et al.* , 2011). Importantly, greater subcortical atrophy in bvFTD can result in severe memory disturbance at presentation (Graham *et al.* , 2005). This raises the possibility that more severe episodic memory and hippocampal atrophy may be a potential biomarker for FTLD-TDP *in vivo* (Josephs *et al.* , 2011).

Glenda Halliday 10/6/12 5:18 PM
Deleted: s

Glenda Halliday 10/6/12 5:19 PM
Deleted: the

Glenda Halliday 10/6/12 5:19 PM
Deleted: s

Glenda Halliday 10/4/14 9:53 AM
Comment: Delete this?

While degeneration of the fornix is a feature of AD (Copenhaver *et al.* , 2006, Mielke *et al.* , 2009), the status of the fornix has not been previously studied in bvFTD, despite knowledge of hippocampal involvement. A recent DTI study in healthy participants confirmed that white matter integrity of the fornix is closely associated with memory recollection (Rudebeck *et al.* , 2009). Our findings show a greater degree of degeneration in this vital white matter tract in bvFTD than in AD, consistent with recent *in vivo* DTI studies showing substantial white matter degeneration in bvFTD (e.g. Whitwell *et al.* , 2010, Zhang *et al.* , 2009). However, the

difference in damage to the fornix is somewhat puzzling considering that hippocampal atrophy was similar in both bvFTD and AD. Although fornix integrity can be reliably measured via DTI (Hua *et al.* , 2008, Mori *et al.* , 2008, Wakana *et al.* , 2007), anatomical analyses of the composition of the fornix has recently shown that this fiber tract does not just contain efferent hippocampal fibres to the mammillary bodies and anterior thalamus, but also contains efferent anterior thalamic fibres back to the hippocampus (Aggleton *et al.* , 2011, Aggleton *et al.* , 2010). As we found atrophy of the anterior thalamus in both the clinical and *postmortem* FTD cohorts but not in AD, these data suggest that bvFTD cases have disconnection of both pathways travelling within the fornix, while AD without substantive anterior thalamic involvement have hippocampal efferent fibers primarily affected. Thalamic atrophy has been reported recently in FTD (Cardenas *et al.* , 2007, Chow *et al.* , 2008, Garibotto *et al.* , 2011), particularly in cases which have subsequently been shown to have TDP pathology at *postmortem* (Rohrer *et al.* , 2010). Our data confirm this concept, but show that both FTLD-TDP and FTLD-tau *postmortem* cases have thalamic and hippocampal atrophy, although those with TDP pathology have greater hippocampal loss. This finding suggests that the thalamus is affected early in both pathological forms of bvFTD, contributing to the greater damage to the fornix, and that over time progressive degeneration to the hippocampus is more TDP-43 dependent in bvFTD.

Glenda Halliday 9/6/12 8:14 PM
Deleted:

Interestingly, in the clinical cohort we did not observe mammillary body atrophy in either disease group, or thalamic atrophy in the AD group. In addition, substantive mammillary body atrophy was not observed in pathologically-confirmed cases with AD (Table 2). This result was unexpected given the substantial fornix degeneration observed using DTI in both bvFTD and AD, and the atrophy of these structures shown in previous *in vivo* studies in AD (Callen *et al.* , 2001, Copenhaver *et al.* , 2006). Methodological differences are likely to contribute to our findings, including the possibility that amnesic FTD cases have been included in some previous AD studies, particularly considering our *postmortem* confirmed volumetric results. Previous

studies of mammillary body and thalamic atrophy in AD (Callen *et al.* , 2001, Copenhaver *et al.* , 2006) were conducted using region of interest manual tracing on scans and did not employ the automated VBM imaging methods used in the present analysis. VBM uses spatial smoothing to make valid cross-subject and group comparisons, and the current data were smoothed with a Gaussian kernel of 3mm which reduces the spatial resolution substantially for smaller regions such as the mammillary bodies. This, in association with the timing of evaluations (thalamic atrophy has been linked to disease progression in AD (Chetelat *et al.* , 2005)), may explain the differences in results obtained between studies. Importantly, the same method of region of interest manual tracing of brain slices was performed in our *postmortem* cohort, showing substantial atrophy of the mammillary bodies and anterior thalamus only in bvFTD, with no substantive differences between pathological subtypes (TDP vs. tau). In contrast, the AD patients showed mammillary body volumes similar to age-matched controls with a minor reduction in the thalamus (~10%) that was not statistical significant (Table 2). No studies of mammillary body atrophy *postmortem* in AD have been published since consensus was achieved for differentiating common dementia syndromes (McKeith *et al.* , 2005, McKhann *et al.* , 2001), and *postmortem* studies of thalamic atrophy in AD have not been conducted to date. In earlier *postmortem* studies, high variability in mammillary body measurements were found (Hooper and Vogel, 1976, Wilkinson and Davies, 1978), with both age and dementia accompanied by a loss of mammillary body volume without neuronal loss (Wilkinson and Davies, 1978) or neuronal atrophy (Ishunina *et al.* , 2003). Only 60% of earlier AD cases reported had senile plaques or neurofibrillary tangles in the mammillary bodies (Grossi *et al.* , 1989, McDuff and Sumi, 1985). These data and the data presented in this study suggest that in AD the mammillary bodies (and by analogy the anterior thalamus) have a variable loss of hippocampal afferents and variable neuronal pathology in the absence of significant neuronal loss.

Glenda Halliday 10/4/14 9:53 AM
Comment: Now have more mam bod atrophy in type A TDP, and Pick's disease having worse thalamic atrophy

Direct comparison of the dementia groups showed more fornix, anterior thalamus and anterior cingulate atrophy in bvFTD than in AD, while the degree of atrophy in the posterior cingulate cortex was not significantly different when the whole bvFTD group was included. The anterior thalamus is the major relay to the anterior cingulate cortex in Papez circuit, and as discussed above, also sends fibers through the fornix to the hippocampus, linking degeneration in these three sites. Our *in vivo* findings of differential damage in these sites were further corroborated by our *postmortem* findings, which again showed greater thalamic and cingulate atrophy in bvFTD. However, splitting the clinical bvFTD cohort into those with more or less memory impairment revealed that AD patients had significantly greater atrophy of the posterior cingulate cortex than bvFTD patients with memory impairment, while memory impaired bvFTD had greater damage in the fornix, anterior thalamus and anterior cingulate gyrus (similar to differences observed in the entire cohort). Previous studies have shown a selective involvement of the posterior cingulate in AD compared with bvFTD (Frisoni *et al.* , 2002, Killiany *et al.* , 2000), consistent with these findings, while studies recently challenging this concept (Barnes *et al.* , 2007) may have studied a bvFTD cohort at later disease stages. Importantly, bvFTD with limited memory impairment had less hippocampal and anterior thalamic atrophy than those with significant memory impairment, suggesting that significant damage to these regions is most important for memory impairment in bvFTD. Overall, our *in vivo* and *postmortem* results indicate that anterior cingulate atrophy is a strong predictor of bvFTD, and that greater hippocampal and thalamic atrophy occurs in bvFTD cases with significant memory impairment.

Glenda Halliday 10/6/12 5:27 PM
Deleted: are likely to

Glenda Halliday 10/6/12 5:27 PM
Deleted: more clinically variable

Taken together, our findings demonstrate that a greater number of subregions in the Papez circuit are affected in clinical and pathological bvFTD compared with AD. Nevertheless, there are several limitations to our approach. In particular, the clinical and pathological samples were from different patient cohorts and thus our findings need to be replicated in a clinical sample that has been followed-up until post-mortem. Similarly, our group sizes were small and

therefore replication of our results in a bigger sample would further strengthen our findings.

Perhaps not surprisingly, our clinical findings further corroborate the notion in the literature that bvFTD patients can show episodic memory deficits of a similar severity to AD, and we suggest that diagnostic exclusion of bvFTD on grounds of memory performance alone should be considered carefully as poor memory does not preclude a FTLD diagnosis. Our data show that damage to the Papez circuit and memory impairment are related, as predicted, and that it is the severity of damage to the anterior thalamus in bvFTD that differentiates memory impaired bvFTD patients from AD and other patients with bvFTD. Importantly, future research should focus on identifying specific “thalamic” memory deficits in these cohorts.

Funding

This work was supported by the Australian Research Council [DP110104202 to M.H., FF0776229 to J.R.H.]; and the National Health and Medical Research Council of Australia [APP1022684 to O.P., 630434 to G.H.].

Acknowledgments

We would like to thank the participants and their families, especially those who donated their brain tissue after death. Data for the clinical study was obtained from FRONTIER clinic at Neuroscience Research Australia, which is funded by an Australian Research Council Centre of Excellence grant and National Health and Medical Research Council of Australia grants. Data for the *postmortem* study was obtained from the Sydney Brain Bank, which is supported by Neuroscience Research Australia, the University of New South Wales and the National Health and Medical Research Council of Australia (NHMRC). The authors report no conflicts of interest or disclosures. We wish to thank the staff of FRONTIER and the Sydney Brain Bank for their assistance, Shelley Forrest for performing the interrater histological quantitation and Heidi Cartwright for assistance with the figurework.

References

Aggleton JP, Brown MW. Episodic memory, amnesia, and the hippocampal-anterior thalamic axis. Behav Brain Sci. 1999; 22(3): 425-44; discussion 44-89.

Aggleton JP, Dumont JR, Warburton EC. Unraveling the contributions of the diencephalon to recognition memory: a review. Learn Mem. 2011; 18(6): 384-400.

Aggleton JP, O'Mara SM, Vann SD, Wright NF, Tsanov M, Erichsen JT. Hippocampal-anterior thalamic pathways for memory: uncovering a network of direct and indirect actions. Eur J Neurosci. 2010; 31(12): 2292-307.

Ashburner J, Friston KJ. Voxel-based morphometry--the methods. Neuroimage. 2000; 11(6 Pt 1): 805-21.

Barnes J, Godbolt AK, Frost C, Boyes RG, Jones BF, Scahill RI, et al. Atrophy rates of the cingulate gyrus and hippocampus in AD and FTLD. Neurobiol Aging. 2007; 28(1): 20-8.

Boccardi M, Laakso MP, Bresciani L, Galluzzi S, Geroldi C, Beltramello A, et al. The MRI pattern of frontal and temporal brain atrophy in fronto-temporal dementia. Neurobiol Aging. 2003; 24(1): 95-103.

Braak H, Braak E. Neuropathological stageing of Alzheimer-related changes. Acta Neuropathologica. 1991a; 82: 239-59.

Braak H, Braak E. Neuropathological staging of Alzheimer-related changes. Acta neuropathol. 1991b; 82: 239-59.

Broe M, Hodges JR, Schofield E, Shepherd CE, Kril JJ, Halliday GM. Staging disease severity in pathologically confirmed cases of frontotemporal dementia. Neurology. 2003; 60(6): 1005-11.

Callen DJ, Black SE, Gao F, Caldwell CB, Szalai JP. Beyond the hippocampus: MRI volumetry confirms widespread limbic atrophy in AD. Neurology. 2001; 57(9): 1669-74.

Cardenas VA, Boxer AL, Chao LL, Gorno-Tempini ML, Miller BL, Weiner MW, et al. Deformation-based morphometry reveals brain atrophy in frontotemporal dementia. Archives of neurology. 2007; 64(6): 873-7.

Chetelat G, Landeau B, Eustache F, Mezenge F, Viader F, de la Sayette V, et al. Using voxel-based morphometry to map the structural changes associated with rapid conversion in MCI: a longitudinal MRI study. Neuroimage. 2005; 27(4): 934-46.

Chow TW, Izenberg A, Binns MA, Freedman M, Stuss DT, Scott CJ, et al. Magnetic resonance imaging in frontotemporal dementia shows subcortical atrophy. Dementia and geriatric cognitive disorders. 2008; 26(1): 79-88.

Copenhaver BR, Rabin LA, Saykin AJ, Roth RM, Wishart HA, Flashman LA, et al. The fornix and mammillary bodies in older adults with Alzheimer's disease, mild cognitive impairment, and cognitive complaints: a volumetric MRI study. Psychiatry research. 2006; 147(2-3): 93-103.

de Leon MJ, Convit A, George AE, Golomb J, de Santi S, Tarshish C, et al. In vivo structural studies of the hippocampus in normal aging and in incipient Alzheimer's disease. Ann N Y Acad Sci. 1996; 777: 1-13.

Desikan RS, Segonne F, Fischl B, Quinn BT, Dickerson BC, Blacker D, et al. An automated labeling system for subdividing the human cerebral cortex on MRI scans into gyral based regions of interest. Neuroimage. 2006; 31(3): 968-80.

Frisoni GB, Testa C, Zorzan A, Sabattoli F, Beltramello A, Soininen H, et al. Detection of grey matter loss in mild Alzheimer's disease with voxel based morphometry. J Neurol Neurosurg Psychiatry. 2002; 73(6): 657-64.

Glenda Halliday 9/6/12 8:25 PM
Formatted: Font:+Theme Body

Garibotto V, Borroni B, Agosti C, Premi E, Alberici A, Eickhoff SB, et al. Subcortical and deep cortical atrophy in Frontotemporal Lobar Degeneration. Neurobiol Aging. 2011; 32(5): 875-84.
Good CD, Johnsrude IS, Ashburner J, Henson RN, Friston KJ, Frackowiak RS. A voxel-based morphometric study of ageing in 465 normal adult human brains. Neuroimage. 2001; 14(1 Pt 1): 21-36.
Graham A, Davies R, Xuereb J, Halliday G, Kril J, Creasey H, et al. Pathologically proven frontotemporal dementia presenting with severe amnesia. Brain. 2005; 128(Pt 3): 597-605.
Grossi D, Lopez OL, Martinez AJ. Mamillary bodies in Alzheimer's disease. Acta Neurol Scand. 1989; 80(1): 41-5.
Grossman M, McMillan C, Moore P, Ding L, Glosser G, Work M, et al. What's in a name: voxel-based morphometric analyses of MRI and naming difficulty in Alzheimer's disease, frontotemporal dementia and corticobasal degeneration. Brain. 2004; 127(Pt 3): 628-49.
Halliday GM, Double KL, Macdonald V, Kril JJ. Identifying severely atrophic cortical subregions in Alzheimer's disease. Neurobiol Aging. 2003; 24(6): 797-806.
Hooper WM, Vogel FS. The limbic system in Alzheimer's disease. American Journal of Pathology. 1976; 85: 1-19.
Hornberger M, Piguet O, Graham AJ, Nestor PJ, Hodges JR. How preserved is episodic memory in behavioral variant frontotemporal dementia? Neurology. 2010; 74(6): 472-9.
Hua K, Zhang J, Wakana S, Jiang H, Li X, Reich DS, et al. Tract probability maps in stereotaxic spaces: analyses of white matter anatomy and tract-specific quantification. Neuroimage. 2008; 39(1): 336-47.
Ishunina TA, Kamphorst W, Swaab DF. Changes in metabolic activity and estrogen receptors in the human medial mamillary nucleus: relation to sex, aging and Alzheimer's disease. Neurobiol Aging. 2003; 24(6): 817-28.
Jack CR, Jr., Petersen RC, Xu YC, Waring SC, O'Brien PC, Tangalos EG, et al. Medial temporal atrophy on MRI in normal aging and very mild Alzheimer's disease. Neurology. 1997; 49(3): 786-94.
Josephs KA, Hodges JR, Snowden JS, Mackenzie IR, Neumann M, Mann DM, et al. Neuropathological background of phenotypical variability in frontotemporal dementia. Acta Neuropathol. 2011; 122(2): 137-53.
Killiany RJ, Gomez-Isla T, Moss M, Kikinis R, Sandor T, Jolesz F, et al. Use of structural magnetic resonance imaging to predict who will get Alzheimer's disease. Annals of neurology. 2000; 47(4): 430-9.
Kril JJ, Halliday GM. Clinicopathological staging of frontotemporal dementia severity: correlation with regional atrophy. Dementia and geriatric cognitive disorders. 2004; 17(4): 311-5.
Kril JJ, Macdonald V, Patel S, Png F, Halliday GM. Distribution of brain atrophy in behavioral variant frontotemporal dementia. J Neurol Sci. 2005; 232(1-2): 83-90.
Mackenzie IR, Neumann M, Bigio EH, Cairns NJ, Alafuzoff I, Kril J, et al. Nomenclature and nosology for neuropathologic subtypes of frontotemporal lobar degeneration: an update. Acta Neuropathol. 2010; 119(1): 1-4.
McDuff T, Sumi SM. Subcortical degeneration in Alzheimer's disease. Neurology. 1985; 35(1): 123-6.
McKeith IG, Dickson DW, Lowe J, Emre M, O'Brien JT, Feldman H, et al. Diagnosis and management of dementia with Lewy bodies: third report of the DLB Consortium. Neurology. 2005; 65(12): 1863-72.

McKhann G, Drachman D, Folstein M, Katzman R, Price D, Stadlan EM. Clinical diagnosis of Alzheimer's disease: report of the NINCDS-ADRDA Work Group under the auspices of Department of Health and Human Services Task Force on Alzheimer's Disease. Neurology. 1984; 34(7): 939-44.
McKhann GM, Albert MS, Grossman M, Miller B, Dickson D, Trojanowski JQ. Clinical and pathological diagnosis of frontotemporal dementia: report of the Work Group on Frontotemporal Dementia and Pick's Disease. Archives of neurology. 2001; 58(11): 1803-9.
Mielke MM, Kozauer NA, Chan KC, George M, Toroney J, Zerrate M, et al. Regionally-specific diffusion tensor imaging in mild cognitive impairment and Alzheimer's disease. Neuroimage. 2009; 46(1): 47-55.
Milner B, Penfield W. The effect of hippocampal lesions on recent memory. Trans Am Neurol Assoc. 1955; (80th Meeting): 42-8.
Mirra SS, Heyman A, McKeel D, Sumi SM, Crain BJ, Brownlee LM, et al. The Consortium to Establish a Registry for Alzheimer's Disease (CERAD). Part II. Standardization of the neuropathologic assessment of Alzheimer's disease. Neurology. 1991; 41(4): 479-86.
Mori S, Oishi K, Jiang H, Jiang L, Li X, Akhter K, et al. Stereotaxic white matter atlas based on diffusion tensor imaging in an ICBM template. Neuroimage. 2008; 40(2): 570-82.
Mori S, Wakana S, Nagae-Poetscher LM, van Zijl PC. MRI atlas of human white matter. Amsterdam: Elsevier; 2005.
Pennington C, Hodges JR, Hornberger M. Neural Correlates of Episodic Memory in Behavioral Variant Frontotemporal Dementia. J Alzheimers Dis. 2011.
Piguet O, Petersen A, Yin Ka Lam B, Gabery S, Murphy K, Hodges JR, et al. Eating and hypothalamus changes in behavioral-variant frontotemporal dementia. Annals of neurology. 2011; 69(2): 312-9.
Rabinovici GD, Seeley WW, Kim EJ, Gorno-Tempini ML, Rascovsky K, Pagliaro TA, et al. Distinct MRI atrophy patterns in autopsy-proven Alzheimer's disease and frontotemporal lobar degeneration. Am J Alzheimers Dis Other Demen. 2007; 22(6): 474-88.
Rascovsky K, Hodges JR, Knopman D, Mendez MF, Kramer JH, Neuhaus J, et al. Sensitivity of revised diagnostic criteria for the behavioural variant of frontotemporal dementia. Brain. 2011.
Rohrer JD, Geser F, Zhou J, Gennatas ED, Sidhu M, Trojanowski JQ, et al. TDP-43 subtypes are associated with distinct atrophy patterns in frontotemporal dementia. Neurology. 2010; 75(24): 2204-11.
Rudebeck SR, Scholz J, Millington R, Rohenkohl G, Johansen-Berg H, Lee AC. Fornix microstructure correlates with recollection but not familiarity memory. J Neurosci. 2009; 29(47): 14987-92.
Seeley WW, Crawford R, Rascovsky K, Kramer JH, Weiner M, Miller BL, et al. Frontal paralimbic network atrophy in very mild behavioral variant frontotemporal dementia. Archives of neurology. 2008; 65(2): 249-55.
van de Pol LA, Hensel A, van der Flier WM, Visser PJ, Pijnenburg YA, Barkhof F, et al. Hippocampal atrophy on MRI in frontotemporal lobar degeneration and Alzheimer's disease. J Neurol Neurosurg Psychiatry. 2006; 77(4): 439-42.
Wakana S, Caprihan A, Panzenboeck MM, Fallon JH, Perry M, Gollub RL, et al. Reproducibility of quantitative tractography methods applied to cerebral white matter. Neuroimage. 2007; 36(3): 630-44.
Whitwell JL, Avula R, Senjem ML, Kantarci K, Weigand SD, Samikoglu A, et al. Gray and white matter water diffusion in the syndromic variants of frontotemporal dementia. Neurology. 2010; 74(16): 1279-87.

Glenda Halliday 9/6/12 8:25 PM
Formatted: Font:+Theme Body

Whitwell JL, Przybelski SA, Weigand SD, Ivnik RJ, Vemuri P, Gunter JL, et al. Distinct anatomical subtypes of the behavioural variant of frontotemporal dementia: a cluster analysis study. Brain. 2009; 132(Pt 11): 2932-46.
Wilkinson A, Davies I. The influence of age and dementia of the neurone population of the mammillary bodies. Age and ageing. 1978; 7(3): 151-60.
Zhang Y, Schuff N, Du AT, Rosen HJ, Kramer JH, Gorno-Tempini ML, et al. White matter damage in frontotemporal dementia and Alzheimer's disease measured by diffusion MRI. Brain. 2009; 132(Pt 9): 2579-92.

Figure Legends

Figure 1. Schematic diagram of the Papez circuit regions.

Figure 2. Voxel-based morphometry and diffusion tensor imaging analyses showing grey matter atrophy and white matter degeneration for the hippocampus and fornix, respectively. Clusters are overlaid on the MNI standard brain (t=2.41). Colored voxels show regions that were significant in the analyses for p<0 .001 uncorrected and a cluster threshold of 20 contiguous voxels.

Figure 3. Voxel-based morphometry analyses showing grey matter atrophy for the anterior thalamus and cingulate cortex. Clusters are overlaid on the MNI standard brain (t=2.41). Colored voxels show regions that were significant in the analyses for p<0 .001 uncorrected and a cluster threshold of 20 contiguous voxels.

Figure 4. Voxel-based morphometry and diffusion tensor imaging analyses showing grey matter atrophy and white matter degeneration for: i) more (bvFTD+) versus less (bvFTD-) memory impaired bvFTD patients; ii) more (bvFTD+) memory impaired bvFTD versus AD patients. Clusters are overlaid on the MNI standard brain (t=2.41). Colored voxels show regions that were significant in the analyses for p<0 .001 uncorrected and a cluster threshold of 20 contiguous voxels.

Figure 5. Micrographs of immunohistochemically-identified inclusions in the CA1 region (**A,B**) and dentate gyrus (**C-F**) of the hippocampus.

A,B Tau-immunoreactive inclusions in the CA1 region of a case of AD (**A**) and Pick's disease (PiD, **B**). Sections counterstained with cresyl violet. Scale in B equivalent for A. A similar density of tau-immunoreactive CA1 inclusions was observed in corticobasal degeneration (CBD, not shown). Very rare TDP-43-immunoreactive inclusions were found in the CA1 region of some bvFTD-TDP cases (not shown).

C-F The dentate gyrus is a predeliction site for inclusions in cases with bvFTD with few inclusions found in this region in AD (not shown). Higher densities of tau-immunoreactive inclusions in the dentate gyrus were observed in cases with CBD (**C**) and PiD (**D**) compared with TDP-43-immunoreactive inclusions in cases with Type A (**E**) or Type C (**F**) pathology. Inset shows the morphology of these inclusions at higher magnification. Sections counterstained with cresyl violet. Scales in F equivalent for C-E. Scale in inset = 10µm.

Glenda Halliday 9/6/12 11:34 PM
Formatted: Font:Not Bold

Glenda Halliday 9/6/12 11:36 PM
Formatted: Font:Not Bold

Glenda Halliday 9/6/12 8:16 PM
Deleted:

Table 1. Mean scores (standard deviation) for bvFTD, AD patients and controls on demographics and cognitive tests.

	In vivo cohort			*Postmortem* cohort		
Demographics & Cognitive Tests (max score)	***bvFTD***	***AD***	***Controls***	***bvFTD***	***AD***	**Controls**
N	15	19	18	19	18	20
Sex (M/F)	10/5	13/6	9/9	9/10	9/9	10/10
Mean age (years)	59 (8)	64 (8)	65 (5)	69 (8)	78 (8)	75 (14)
Length of disease (years)	3.7 (2.6)	2.7 (1.7)	-	5.6 (3.6)	5.9 (3.2)	-
Path stage (4 # or 6 @)	-	-	-	2.8 (0.7) #	5.7 (0.6) @	0.85 (1.4) @
ACE (100)	75.6 (11.4) *	80.1 (11.4) *	95.4 (2.9)	-	-	-
RAVLT A6 (15)	3.2 (3.3) *	3.9 (2.9) *	9.6 (1.8)	-	-	-
RAVLT recognition (15)	11.7 (5.5)	10.1 (3.6)	13.2 (3)	-	-	-
Rey Figure 3min recall (36)	5.6 (5.2) *	5.1 (4.5) *	19 (6.5)	-	-	-
Doors & People A (12)	7.8 (2.5) *	7.9 (2.4) *	10.7 (1)	-	-	-

Pathological staging for FTD (Broe *et al.* 2003). @ Pathological staging for AD and aged controls. *p<0.001 disease groups different from controls.

Glenda Halliday 9/6/12 8:22 PM
Deleted: XXX

Glenda Halliday 9/6/12 8:21 PM
Deleted: XX

Glenda Halliday 9/6/12 8:26 PM
Deleted: XX

Glenda Halliday 9/6/12 8:28 PM
Deleted: XX

Glenda Halliday 9/6/12 8:25 PM
Formatted: Highlight

Glenda Halliday 9/6/12 8:27 PM
Formatted: Highlight

Table 2. Mean regional volumes (standard error) for the *postmortem* control group, with covariate-adjusted percentages of regional control volume (standard error) found in AD, bvFTD and bvFTD subgroups.

Region	Controls (mm^3)	AD (% control volume)	bvFTD (% control volume)	bvFTD-TDP (% control volume)	bvFTD-tau (% control volume)	FTD-TDP A (% control volume)	FTD-TDP C (% control volume)	FTD-tau PiD (% control volume)	FTD-tau CBD (% control volume)
Hippocampus	4025 (110)	67 (3)*	55 (3)*#	51 (4)*#	58 (3)*#	49 (5)*#	52 (6)*#	53 (4)*#	67 (6)*
Mammillary bodies	75 (3)	100 (5)	67 (5)*	54 (8)*#	72 (7)*#	46 (11)*#@	63 (13)*#	63 (8)*#	86 (13)*#
Anterior thalamus	1802 (68)	88 (5)	61 (5)*	67 (7)*#	55 (6)*#	69 (10)*	65 (12)*	50 (8)*#	66 (12)*
Cingulate	11000 (223)	80 (2)*	60 (2)*#	61 (4)*#	59 (3)*#	65 (5)*#	59 (6)*#	56 (4)*#	63 (6)*#
Anterior Cingulate	6107 (152)	85 (3)*	58 (3)*#	65 (5)*#&	51 (4)*#	62 (7)*#	71 (8)*#	44 (5)*#^	66 (8)*#
Posterior Cingulate	4893 (118)	78 (3)*	63 (3)*#	61 (5)*#	64 (4)*#	68 (6)*	56 (7)*#	63 (5)*#	62 (7)*#

*p<0.001 disease groups different from controls

Glenda Halliday 10/6/12 8:57 AM
Formatted Table

Glenda Halliday 10/6/12 8:15 AM
Deleted:

Glenda Halliday 10/6/12 8:30 AM
Deleted: 0…3…& … [1]

Glenda Halliday 10/6/12 8:31 AM
Deleted: 60…7… … [2]

Glenda Halliday 10/6/12 8:31 AM
Deleted: 5…5… … [3]

Glenda Halliday 10/6/12 8:27 AM
Deleted: 3… … [4]

Glenda Halliday 10/6/12 8:28 AM
Deleted: 1… … [5]

Glenda Halliday 10/6/12 8:28 AM
Deleted: 2… … [6]

[#]p<0.001 bvFTD different from AD

[&]p<0.01 bvFTD-TDP different from bvFTD-tau

[@]p<0.01 bvFTD-TDP different from bvFTD-tau CBD

^p<0.01 different from all other subgroups

Table 3. Mean number of inclusions per mm^3 (standard error) in the bvFTD-tau and bvFTD-TDP subgroups of the *postmortem* cohort.

Hippocampal Region	AD	bvFTD-TDP Total	bvFTD-tau Total	bvFTD-TDP Type A	bvFTD-TDP Type C	bvFTD-tau PiD	bvFTD-tau CBD
CA1	41 (6)	0 (9)[#&]	59 (7)	0 (11)[#]	2 (13)[#]	69 (9)[#^]	27 (13)
Dentate average	9 (18)	58 (26)[&]	261 (22)[#]	60 (25)	49 (30)	338 (20)[#^]	67 (30)[#]
Dentate highest	62 (44)	176 (65)[&]	515 (56)[#]	229 (79)	94 (93)	626 (61)[#^]	255 (92)[#]

[#]p<0.001 bvFTD different from AD

[&]p<0.01 bvFTD-TDP different from bvFTD-tau

^p<0.01 different from all other subgroups

Glenda Halliday 9/6/12 10:57 PM
Deleted:

Glenda Halliday 10/6/12 9:59 AM
Formatted: Superscript

Glenda Halliday 9/6/12 11:15 PM
Formatted: Font:12 pt

Glenda Halliday 9/6/12 11:15 PM
Formatted: Font:12 pt

Glenda Halliday 10/6/12 10:01 AM
Formatted Table

Glenda Halliday 9/6/12 10:57 PM
Deleted:

Glenda Halliday 10/6/12 10:07 AM
Deleted:

Supplementary table 1. Mean scores (standard deviation) for bvFTD, AD patients and controls in the clinical cohort for background neuropsychological tests.

	AD	bvFTD	Control	*KW*	AD vs. bvFTD	AD vs. Control	bvFTD vs. Control
ACE-R							
Attention	15.72 (2.74)	15.33 (2.53)	17.67 (.59)	**	n.s.	**	**
Memory	15.94 (4.45)	18.00 (4.69)	24.11 (1.81)	***	n.s.	***	***
Fluency	8.28 (3.94)	5.60 (3.48)	12.28 (1.53)	***	*	***	***
Language	22.83 (3.45)	22.53 (2.50)	25.22 (1.00)	***	n.s.	**	***
Visuospatial	14.06 (2.51)	14.27 (2.19)	15.72 (.57)	*	n.s.	*	*
Total	76.83 (14.08)	75.73 (8.71)	95.00 (3.38)	***	n.s.	***	***
VOSP							
Dot	9.71 (.47)	9.18 (1.83)	9.60 (.89)	n.s.	-	-	-
Position	19.29 (1.38)	18.55 (1.92)	20.00 (.00)	n.s.	-	-	-
Cube	8.08 (1.93)	8.60 (2.17)	9.20 (1.30)	n.s.	-	-	-
Boston Naming Test	12.63 (2.00)	12.47 (1.77)	14.56 (.86)	***	n.s.	**	**
SydBat							
Naming	22.11 (4.48)	21.43 (3.32)	26.39 (2.40)	***	n.s.	**	***
Repetition	28.89 (2.08)	29.57 (.85)	29.76 (.66)	*	n.s.	*	n.s.
Comprehension	26.83 (1.89)	24.14 (4.75)	29.24 (1.68)	***	.059	***	***
Semantic	25.06 (2.46)	21.92 (4.05)	28.06 (1.89)	***	**	**	***

Trails							
A time	69.11 (32.27)	66.67 (31.80)	29.72 (6.09)	***	n.s.	***	***
B Time	160.38 (58.47)	176.90 (105.35)	78.11 (28.45)	***	n.s.	***	***
Digit Span							
Forwards	9.83 (2.48)	8.27 (2.34)	11.39 (2.23)	**	.057	n.s.	**
Backwards	5.78 (1.96)	4.73 (2.31)	8.67 (2.97)	***	n.s.	**	***
Hayling							
Section 1	3.89 (1.60)	3.93 (1.69)	5.67 (1.03)	***	n.s.	**	***
Section 2	4.06 (2.01)	4.07 (2.23)	6.00 (.00)	**	n.s.	**	**
A Errors	1.82 (2.13)	8.64 (5.14)	.28 (.46)	***	***	**	***
B Errors	3.59 (2.50)	2.29 (2.67)	1.06 (1.63)	**	n.s.	**	n.s.
Overall	3.67 (2.03)	2.57 (1.55)	6.33 (.59)	***	n.s.	***	***

Note. KW values indicate differences across diagnostic groups. n.s. = non significant; *** = $p < .000$; ** = $p < .01$; * = $p < .05$.

Figure 1

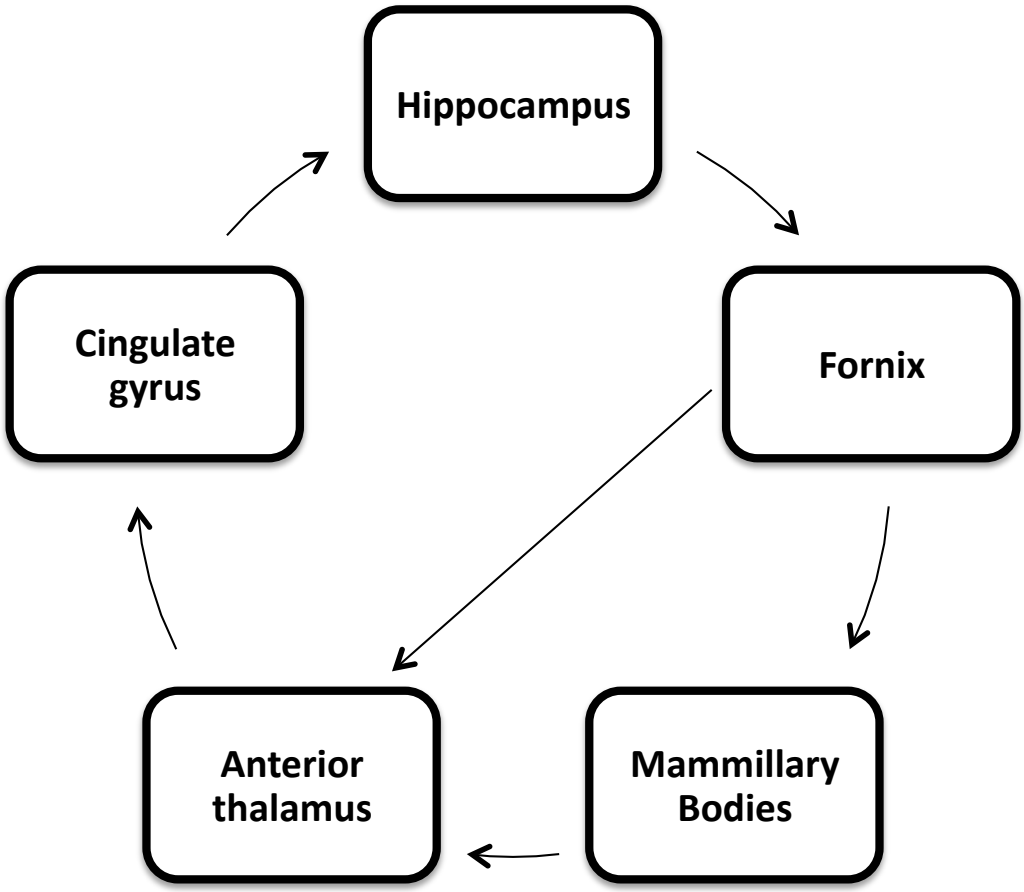
Hippocampus
Fornix
Mammillary Bodies
Anterior thalamus
Cingulate gyrus

Figure 2

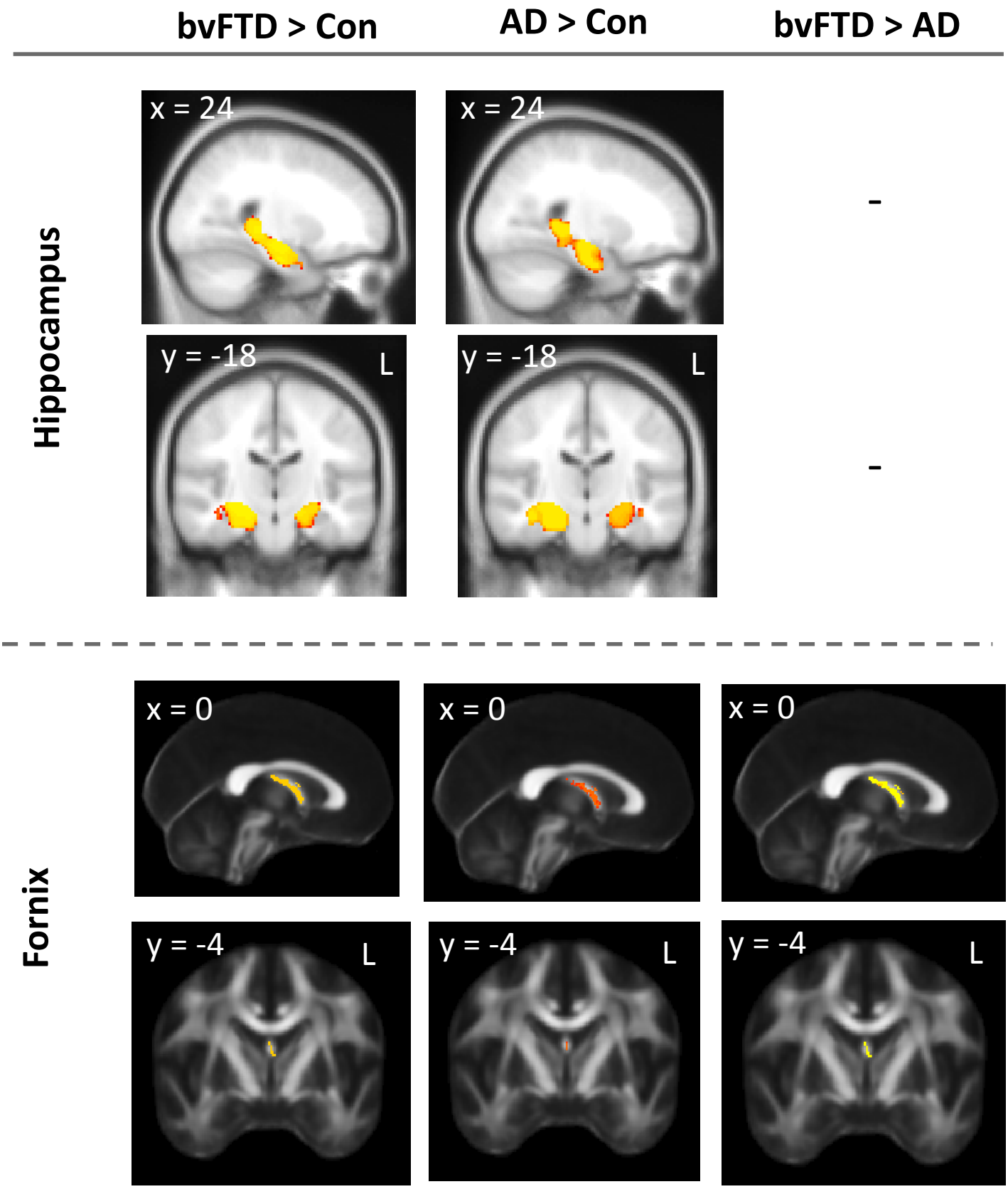
bvFTD > Con
AD > Con
bvFTD > AD
Hippocampus
x = 24
x = 24
-
y = -18
L
y = -18
L
-
Fornix
x = 0
x = 0
x = 0
y = -4
L
y = -4
L
y = -4
L

Figure 3

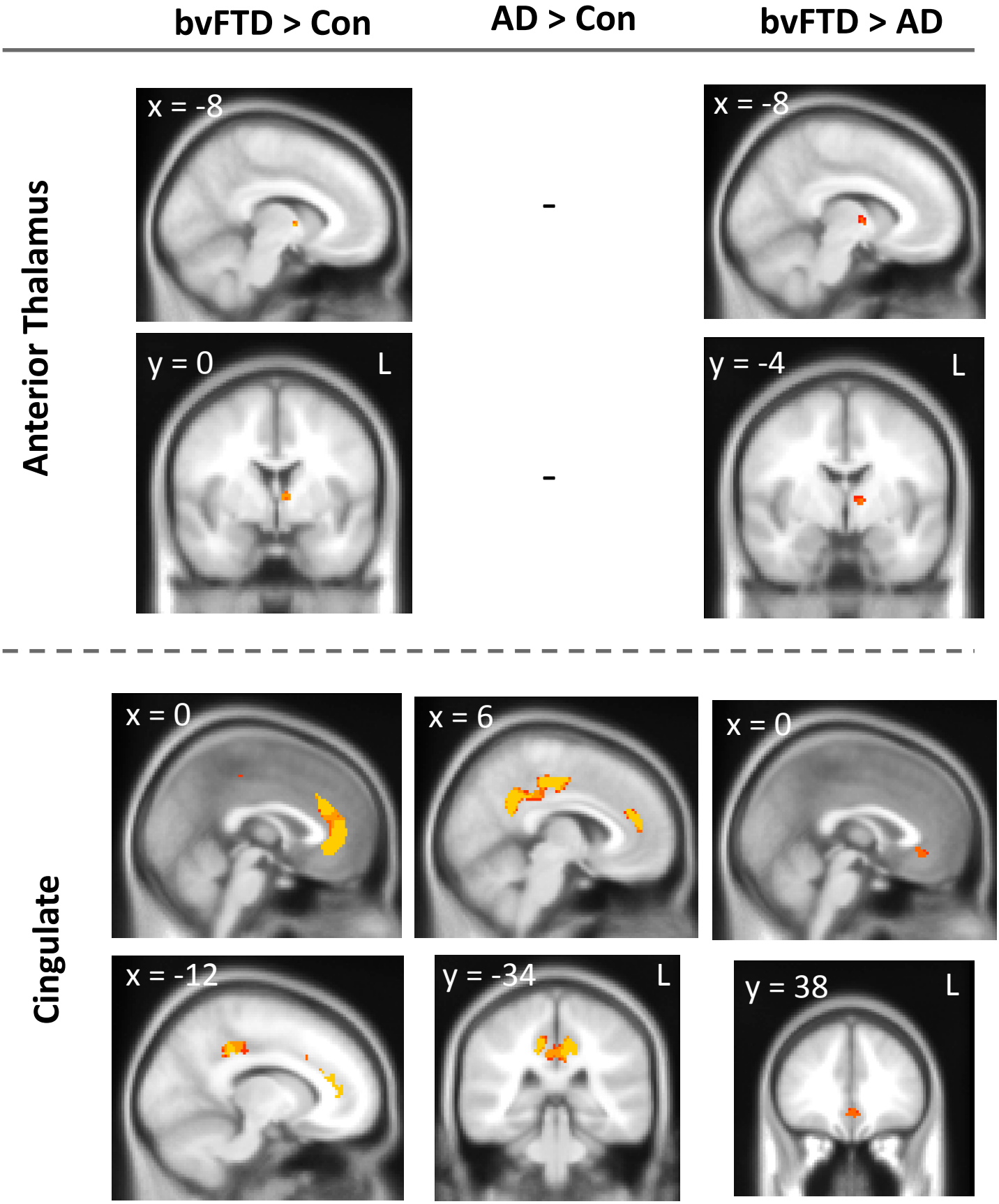
bvFTD > Con
AD > Con
bvFTD > AD
Anterior Thalamus
x = -8
-
x = -8
y = 0
L
-
y = -4
L
Cingulate
x = 0
x = 6
x = 0
x = -12
y = -34
L
y = 38
L

Figure 4

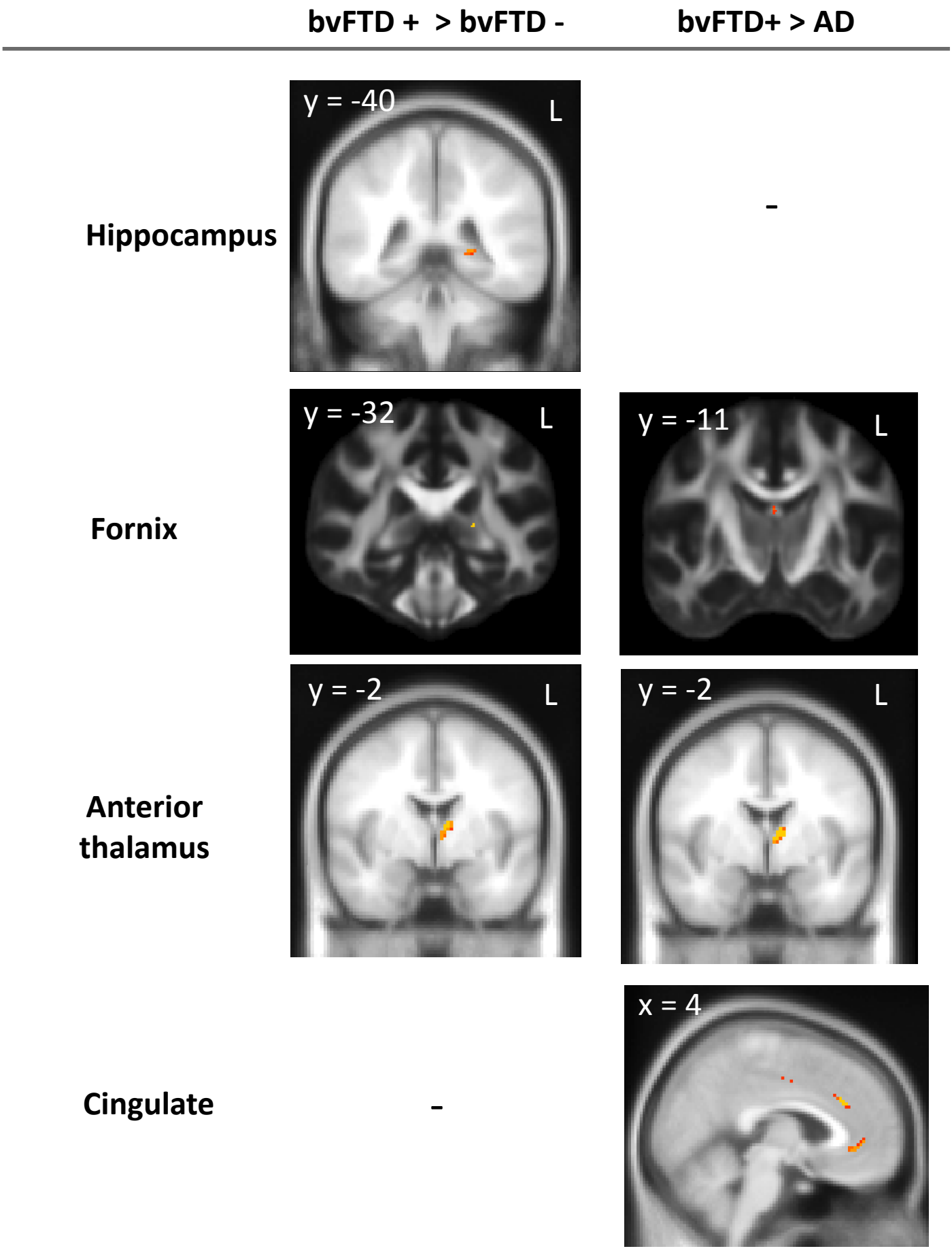
bvFTD + > bvFTD -
bvFTD+ > AD
Hippocampus
y = -40
L
-
Fornix
y = -32
L
y = -11
L
Anterior thalamus
y = -2
L
y = -2
L
Cingulate
-
x = 4